AGU PUBLICATIONS

JGR

Journal of Geophysical Research: Oceans

RESEARCH ARTICLE

10.1002/2015JC011181

Special Section:
Physical Processes Responsible for Material Transport in the Gulf of Mexico for Oil Spill Applications

Time scales in Galveston Bay: An unsteady estuary

Matthew D. Rayson[1,2], Edward S. Gross[1,3], Robert D. Hetland[4], and Oliver B. Fringer[1]

[1]Bob & Norma Street Environmental Fluid Mechanics Laboratory, Department of Civil and Environmental Engineering, Stanford University, Stanford, California, USA, [2]School of Civil, Environmental and Mining Engineering and the Oceans Institute, University of Western Australia, Crawley, Western Australia, Australia, [3]Center for Watershed Sciences, University of California Davis, Davis, California, USA, [4]Department of Oceanography, Texas A & M University, College Station, Texas, USA

Abstract Estuarine time scales including the turnover, particle *e*-folding time, the age (calculated with a passive tracer), and residence time (calculated with Lagrangian particles) were computed using a three-dimensional hydrodynamic model of Galveston Bay, a low-flow, partially stratified estuary. Time scales were computed during a time period when river flow varied by several orders of magnitude and all time scales therefore exhibited significant temporal variability because of the unsteadiness of the system. The spatial distributions of age and residence time were qualitatively similar and increased from 15 days in a shipping channel to >45 days in the upper estuary. Volume-averaged age and residence time decreased during high-flow conditions. Bulk time scales, including the freshwater and salinity turnover times, were far more variable due to the changing river discharge and salt flux through the estuary mouth. A criterion for calculating a suitable averaging time is discussed to satisfy a steady state assumption and to estimate a more representative bulk time scale. When scaled with a freshwater advective time, all time scales were approximately equal to the advective time scale during high-flow conditions and many times higher during low-flow conditions. The mean age, Lagrangian residence, and flushing times exhibited a relationship that was weakly dependent on the freshwater advective time scale demonstrating predictability even in an unsteady, realistic estuary.

Key Points:
- Different time scales calculated in realistic estuary with transient river forcing
- Mean age and Lagrangian residence time exhibit similar spatial and temporal variability
- Time scales showed weak dependence on river flow under highly unsteady conditions

Correspondence to:
M. D. Rayson,
matt.rayson@gmail.com

Citation:
Rayson, M. D., E. S. Gross, R. D. Hetland, and O. B. Fringer (2016), Time scales in Galveston Bay: An unsteady estuary, *J. Geophys. Res. Oceans*, *121*, 2268–2285, doi:10.1002/2015JC011181.

Received 28 JUL 2015
Accepted 29 FEB 2016
Accepted article online 3 MAR 2016
Published online 3 APR 2016

1. Introduction

There are various time scales relevant to physical and biological understanding of an estuary that are often used to characterize a system [*Lucas*, 2010]. Quantifying these time scales is particularly important for understanding the potential exposure and risk from an industrial accident, such as an oil spill. Both bulk, or system wide, and local time scales are useful for predicting transport of material, such as oil, through the system and response of an estuary to variations in forcing, such as a large river flooding event. Bulk time scales include the flushing time, freshwater turnover time, salinity turnover time, and the *e*-folding flushing time of a passive tracer. Bulk time scales treat an estuary as a single box or compartment and therefore do not elucidate any information about spatial variability [*Sheldon and Alber*, 2006]. Local or regionally specific time scales, including the residence time and age, despite being more difficult to generalize, are more representative of the time taken for material to pass through the system. These different time scales are summarized below. The reader should also refer to *Takeoka* [1984], *Monsen et al.* [2002], and *Lucas* [2010] for more thorough discussions of these topics.

1.1. Freshwater Turnover Time: τ_f

The freshwater turnover time is defined as the mean time a tracer remains in an estuary or more specifically "the time required for the freshwater discharge to completely replace the fresh water in the estuarine volume" [*Fischer et al.*, 1979]. Defining the freshwater fraction as

$$f = \frac{s_o - s}{s_o}, \tag{1}$$

where s_o is the ocean salinity, the flushing time is

$$\tau_f = \frac{\int_V f dV}{Q_r}, \tag{2}$$

where Q_r is the freshwater (river) discharge rate and V is the total volume of the estuary. The assumption here is that the discharge is constant in time.

1.2. Salinity Turnover Time: τ_T

The salinity turnover time is the time required for the salt volume to be completely replaced by the incoming salt flux at the mouth, i.e.,

$$\tau_T = \frac{\int_V s\, dV}{\langle F_{in} \rangle}, \tag{3}$$

where $\langle F_{in} \rangle \equiv \langle Q_{in} s_{in} \rangle$ is the residual salt flux into the estuary, Q_{in} and s_{in} are the residual exchange flow and salinities, respectively, and $\langle \cdot \rangle$ is a low-pass filter. A precise definition of the residual salt flux is given in section 2.4. Although *MacCready* [2011] refers to τ_T as the residence time, to be consistent with several authors [e.g., *Tartinville et al*., 1997; *Lucas*, 2010] we will refer to it as the *turnover time*.

1.3. Lagrangian Residence Time: τ_L

The Lagrangian residence time, τ_L, is defined as a time taken for a parcel of fluid to leave an estuary through its mouth [see e.g., *Bolin and Rodhe*, 1973; *Takeoka*, 1984; *Monsen et al*., 2002]. Residence time is therefore a regionally specific time scale. Lagrangian particle tracking techniques may be used to track the *transit time* or *residence time* of individual regions within an estuary. As the origin of each particle is known, spatial maps of residence time can therefore be constructed. Residence time is the complement of age. The key difference between the two is that age is the time a water parcel has spent inside the system since entering, while residence time is the time it takes to leave. Both quantities can be nonstationary; they do not assume a steady state.

1.4. Lagrangian Flushing Time: τ_e

Particles released uniformly, so that each represents the same increment of water volume, can also be used to give a bulk measure of flushing time for an estuary. Fitting a first-order decay function to the number of particles left inside the estuary at time t gives a time scale, τ_e,

$$N(t) = N_0 e^{-t/\tau_e}, \tag{4}$$

where N is the number of particles at any time, N_0 is the initial number of particles, and τ_e is the e-folding flushing time [*Monsen et al*., 2002]. The inherent assumption in using this time scale is that the system behaves as a continuously stirred tank reactor (CSTR), i.e., a well-mixed compartment, whose concentration decreases as a decaying process; the decay process here is analogous to a diffusive flux through the mouth.

1.5. Mean Age

The age represents the amount of time an individual fluid parcel or particle has spent inside of a domain since it entered through the mouth [*Monsen et al*., 2002]. Although age is intrinsically a Lagrangian property, *Delhez et al*. [1999] and *Deleersnijder et al*. [2001] developed the concept of "mean age" useful for evaluating the age in an Eulerian framework, i.e., using a tracer within a numerical model. Age is a spatially and temporally dependent variable that accounts for the time history of a flow field in an estuary, and is therefore useful for characterizing unsteady systems. Previous numerical studies that have used age include *Banas and Hickey* [2005] and *Zhang et al*. [2010] among others.

It is not clear from the literature how these different time scales relate, particularly in an unsteady system that is constantly adjusting to changes in forcing. *Lemagie and Lerczak* [2014] investigated the sensitivity of these bulk and local time scales (except mean age) in Yaquina Bay, Oregon, under the assumption of steady forcing (constant river flow and tidal amplitude). They concluded that the bulk time scales (τ_T and τ_f) are not representative time scales in realistic bays where there is spatial heterogeneity in the tracer field. Here we look at the time scales subject to unsteady forcing in a different estuary, namely Galveston Bay in Texas.

The study site is Galveston Bay, Texas, a wide and shallow (3 m deep) estuary with a 15 m deep, narrow shipping channel running along its length and a narrow entrance to the Gulf of Mexico (Figure 1). Galveston Bay is the busiest petrochemical port in the United States and frequent oil spills are a consequence of this activity. Between 1998 and 2009, there were over 3500 reported spill incidents with a combined volume of 416,000 gal. according to data from the Texas General Land Office [*Lester and Gonzalez*, 2011]. In March

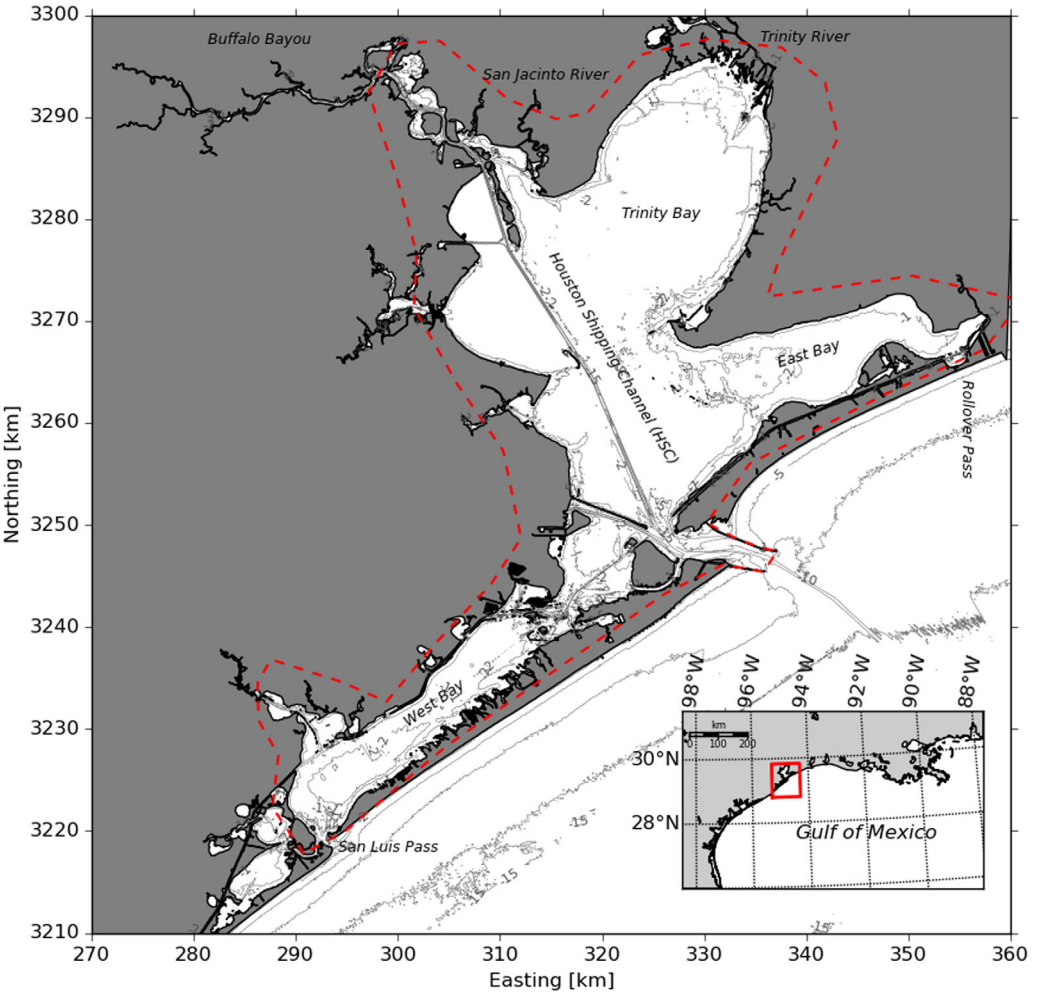

Figure 1. Galveston Bay with 1, 2, 5, 10, and 15 m bathymetry contours shown. Map is projected onto UTM zone 15°N. Dashed red line indicates the boundary of the estuary domain used to calculate the various time scales.

2014, a barge carrying bunker fuel collided near the entrance of the estuary spilling 168,000 gal. This spill is referred to as the Texas City "Y" spill. Monitoring after the incident revealed that much of the oil exited the bay within a day and washed up on the shoreline near Matagorda Bay to the SW of Galveston (response.restoration.noaa.gov). Such a short residence time is indicative of a short transport time scale near the mouth of the estuary owing to strong flushing by tidal currents. While the residence time at the mouth of the bay is relatively short, it can be highly variable throughout the bay. Ultimately, transport time scales determine the exposure risk of different regions of the bay to an oil spill and also may be used to focus resources in the event of a containment.

The purpose of this paper is to calculate each of the aforementioned time scales in Galveston Bay using a three-dimensional hydrodynamic model with realistic forcing conditions and to compare and contrast the results. Although we are focusing on a single estuary, results will be generalizable to other barrier-island lagoon-type estuaries along the Gulf of Mexico coast (e.g., Mobile Bay, Alabama) and the east coast of the United States (e.g., Pamlico Sound, North Carolina) that have long transport time scales of weeks to months and intermittent freshwater inflows. Much of the present understanding of the transport time scales in Gulf estuaries is presented in *Solis and Powell* [1999], who calculated the freshwater turnover time (equation (2)) for several estuaries. They calculated $\tau_f = 40$ days in Galveston Bay based on annual average river discharge. Hydraulic replacement time scales (V/Q_r) ranging between 12 and 88 days have been reported in the literature by *Santschi* [1995] and *Roelke et al.* [2013] based on annual average and extreme river discharge values. We will demonstrate the variability of this time scale and make the conclusion that it is only valid during high river discharge conditions.

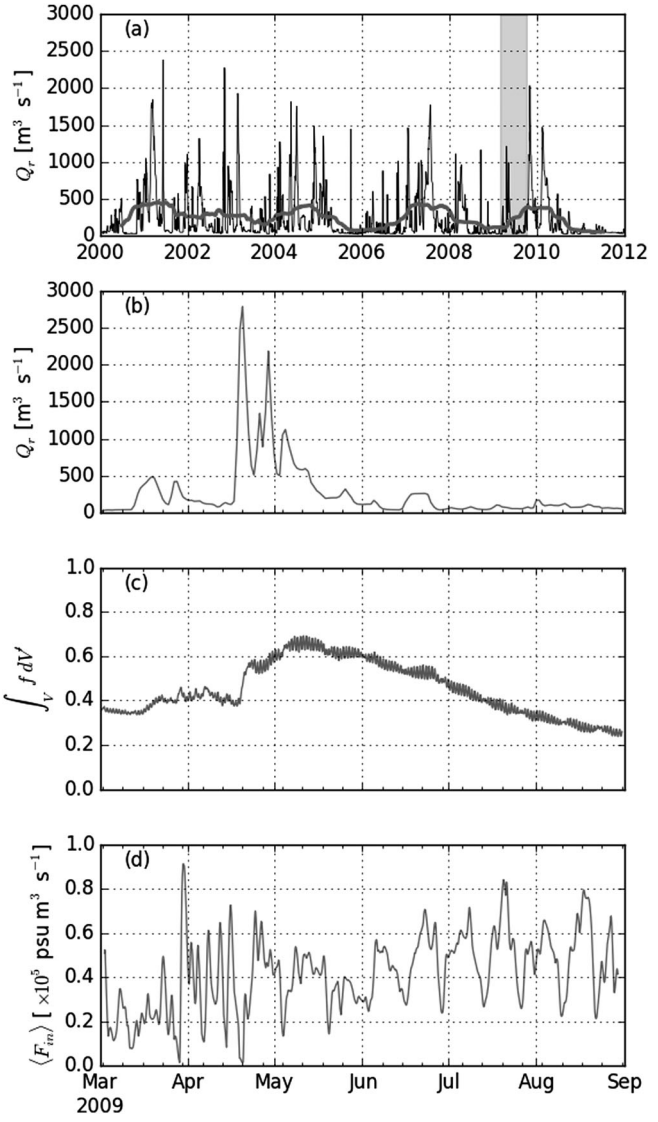

Figure 2. (a) Trinity River flow rate for the period 2000–2012 (black) and the running annual average (gray). (b) Total river discharge, (c) freshwater fraction, and (d) inward salt flux computed from the 2009 SUNTANS simulation. The gray box in Figure 2a indicates the 6 month model hindcast period studied in this paper.

We begin by describing the study site and the methods used to calculate the time scales. The temporally and/or spatially dependent time scales are presented in the results. We then discuss the influence of unsteady forcing and finish by relating the different time scales to river flow.

2. Methodology

2.1. Study Site

The tidal range in Galveston Bay is small (<0.5 m) although the tidal currents through the main entrance exceed 1.0 m s^{-1} [*Rayson et al.*, 2015]. Peak river discharge of 1000–3000 m^3 s^{-1} usually occurs over a period of roughly 1 month or less and is generally preceded by several months of low (∼10 m^3 s^{-1}) discharge (Figure 2a). There is, however, interannual variability in the river discharge with annual averages ranging 50–500 m^3 s^{-1}. The circulation on the Texas-Louisiana shelf, the Mississippi River plume in particular, can drive lower-salinity water (∼24 g kg^{-1}) through the mouth of Galveston Bay. Subtidal water level fluctuations driven by wind stress, barometric effects, remote storm generated Kelvin waves, and mesoscale eddies also drive volume fluxes through the mouth of the estuary. These processes all contribute to the variability of salinity within the estuary [*Rayson et al.*, 2015].

2.2. Model Description

We have used the three-dimensional SUNTANS hydrodynamic model [*Fringer et al.*, 2006] to hindcast a high river discharge event over a 6 month period between March and September 2009 that is representative of typical flow conditions (see Figure 2a). SUNTANS solves the three-dimensional Reynolds-averaged Navier-Stokes equations discretized on an unstructured horizontal grid. We have used the model setup described in *Rayson et al.* [2015], in particular, the *mixed quadrilateral-triangular* grid configuration. This grid consists of 57,305 horizontal grid cells with a median resolution of 100 m in the shipping channel and estuary mouth regions. Twenty fixed z-layers discretized the vertical coordinate. Tidal boundary conditions were prescribed using a blend of gauge data and a Gulf of Mexico regional tidal model that provided spatial tidal amplitude and phase information; temperature and salinity data were interpolated from a shelf-scale ROMS model configuration. Realistic river discharge rates were prescribed from a hydrological model that accounts for gaged and ungaged watersheds that drain into Galveston Bay [*Schoenbaechler and Guthrie*, 2012]. Atmospheric heat, salt, and momentum fluxes were included using data from the North American Regional Reanalysis [*Mesinger et al.*, 2006]. See *Rayson et al.* [2015] for details of the model validation against long-term salinity, water level, temperature, and current monitoring observations.

Rayson et al. [2015] reported accurate prediction of salinity time series at several stations throughout the extent of Galveston Bay with a salinity bias and root-mean-squared error of 1 and 3 psu, respectively. This validation exercise indicates that the model is representing salt transport accurately and is therefore suitable for predicting time scales of variability in the estuary.

2.3. Numerical Implementation of a "Mean" Age Tracer

We will provide a brief overview of the concept of mean age as presented in *Delhez et al.* [1999] and *Deleersnijder et al.* [2001] and its implementation in the SUNTANS numerical model. If a parcel of fluid has concentration $c(t,\ \mathbf{x},\ \tau)$ where τ is the age of the fluid parcel, then the governing equation for the concentration is

$$\frac{\partial c}{\partial t}+\nabla\cdot(\mathbf{u}c)=\frac{\partial}{\partial z}\left(K_T\frac{\partial c}{\partial z}\right)+\frac{\partial c}{\partial \tau}, \tag{5}$$

subject to boundary conditions and assuming that there are no concentration sources or sinks within the domain of interest. The total concentration is then

$$C(t,\ \mathbf{x})=\int_0^\infty c(t,\ \mathbf{x},\ \tau)\ d\tau. \tag{6}$$

The mean age of a parcel of fluid is found by taking the first moment of the total concentration

$$a(t,\ \mathbf{x})=\frac{\alpha(t,\ \mathbf{x})}{C(t,\ \mathbf{x})}, \tag{7}$$

where $C\in[0,\ 1]$ and

$$\alpha(t,\ \mathbf{x})=\int_0^\infty \tau c(t,\ \mathbf{x},\ \tau)\ d\tau, \tag{8}$$

is the age concentration. Given the condition

$$\lim_{\tau\to\infty} c(t,\ \mathbf{x},\ \tau)=0,$$

The governing equations for C and α are

$$\frac{\partial C}{\partial t}+\nabla\cdot(\mathbf{u}C)=\frac{\partial}{\partial z}\left(K_T\frac{\partial C}{\partial z}\right), \tag{9}$$

$$\frac{\partial \alpha}{\partial t}+\nabla\cdot(\mathbf{u}\alpha)=\frac{\partial}{\partial z}\left(K_T\frac{\partial \alpha}{\partial z}\right)+C. \tag{10}$$

The mean age calculation was performed in SUNTANS by solving the transport of two new tracers (C and α) with the existing scalar transport function. We used the higher-order flux limiting scheme for unstructured grids developed by *Casulli and Zanolli* [2005] for scalar transport, details of which are described in *Chua and Fringer* [2011]. Denoting the SUNTANS update of the total concentration as

$$C^{n+1}=\mathcal{A}(C^n),$$

where $\mathcal{A}$ represents the SUNTANS scalar transport (advection-diffusion) solver, the update for the age concentration is given by

$$\alpha^{n+1}=\mathcal{A}(\alpha^n)+\Delta t C^n.$$

The mean age, a, at each grid cell is then evaluated via (7).

The boundary conditions of the concentration tracer at different locations are specified according to the type of question being asked. To determine the water age in an estuary as defined in *Takeoka* [1984], C is set to unity at grid cells along the mouth cross section, and the mean age then evolves based on the model hydrodynamics. In this study, the age concentration tracer, α, was set to zero and the concentration, C, was

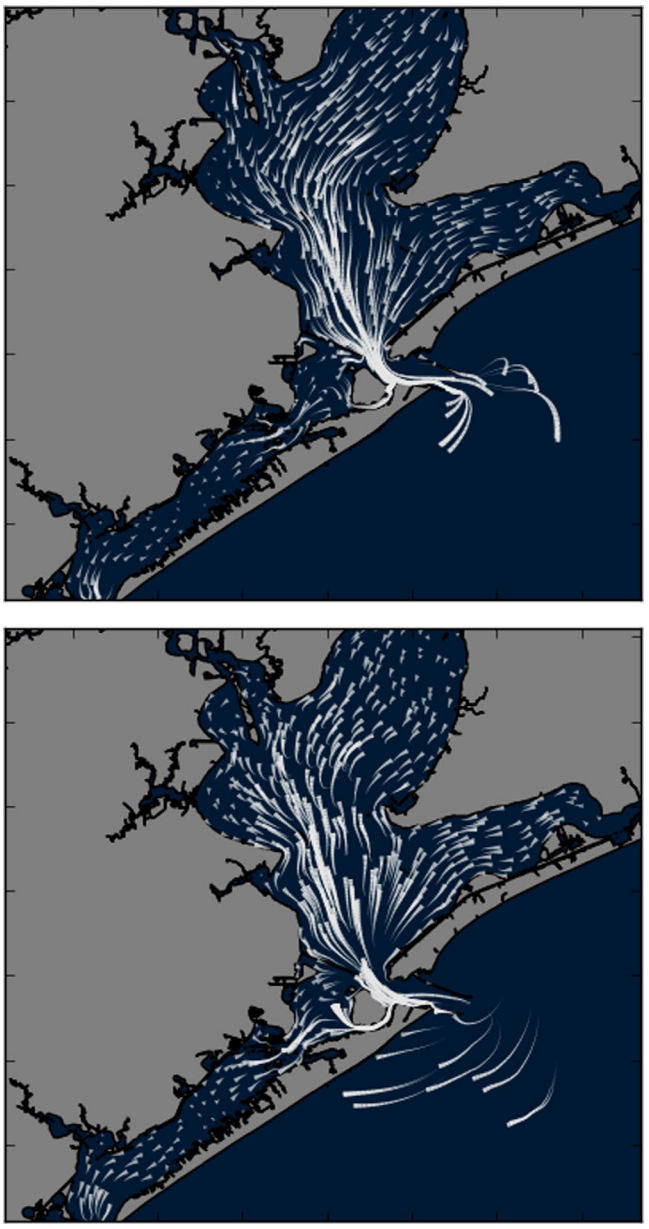

Figure 3. Twelve hour particle path lines during (top) ebb and (bottom) flood phases of the tidal cycle. Only every 37th surface particle is shown for clarity.

set to unity for all of the grid cells crossing the estuary entrance, thereby "aging" all water that flows through this cross section into the bay. Posing the problem in this manner answers the question: how long will a tracer persist in the bay after flowing through the mouth? It is equivalent to the methodology applied by *Banas and Hickey* [2005] to map residence times in Willapa Bay, Washington.

2.4. Particle Tracking Model Description

The Flexible Integration of Staggered-grid Hydrodynamics Particle Tracking Model estimates particle trajectories using three-dimensional hydrodynamic information [*Ketefian et al.*, 2016]. The backward stochastic differential equation of *LaBolle et al.* [1998] was used to estimate particle trajectories. Horizontal advection was estimated by a streamline tracking method that analytically integrates a linear reconstruction of the subgrid-scale velocity field to estimate advective trajectories [*Ketefian et al.*, 2016]. This advection method follows the approach of *Postma et al.* [2013] to reconstruct a local velocity field consistent with the discrete continuity equation thereby avoiding unphysical clustering of particles that can result with particle tracking approaches that do not consider consistency with the discrete continuity equation.

We used the particle trajectories from FISHPTM to calculate the Lagrangian residence time (τ_L) and *e*-folding flushing time (τ_e) for Galveston Bay. To calculate the residence time and the *e*-folding flushing time, particles were initialized on a 250 m $\times$ 250 m uniform grid within the estuary and their positions were integrated forward in time for 45 days, which was deemed suitable based on trial and error of residence time for most parts of the estuary as will be shown in the results. Particles were released at 1 m depth intervals throughout the water column and tracked in three dimensions. Approximately 58,000 particles were initialized at the beginning of each day of the 6-month simulation during March-September 2009. Because particle tracks were computed for 45 days, Lagrangian and *e*-folding flushing times could be computed for all but the last 44 days of the hydrodynamic model simulation period, which ended on 1 September 2014. Figure 3 shows an example of particle trajectories over two different phases of the tidal cycle.

2.4.1. Lagrangian Residence Time Calculation

To calculate τ_L, each particle was assigned an age which was increased in time as long as it remained inside of the polygon surrounding the estuary indicated by the dashed red line in Figure 1. Age was reset to zero

for particles outside of the polygon and only started incrementing again if a particle reentered the estuary. The maximum age attained by each particle was recorded. The Lagrangian residence time, $\tau_L(x_0,\ y_0)$, at each initial particle location is the maximum age attained for that particle. As the particles were initialized on a regular grid, spatial maps of residence time could easily be constructed. Lagrangian residence and flushing times that were calculated were time dependent based on flow conditions.

2.4.2. Lagrangian Flushing Time Calculation

The number of particles in the estuary, $N(t)$, was then used to estimate τ_e via linear regression of (4) in the form

$$\ln\left(N(t)\right) = -t/\tau_e + \ln\left(N_0\right)$$

where $N(t)$ is the number of particles inside of the estuary at time t.

2.5. Isopycnal Salt Flux

Calculating the tracer turnover time via equation (3) requires a suitable estimate of the average salt flux into the estuary, $\langle F_{in}\rangle$. Time-averaged fluxes through an Eulerian cross section do not capture the exchange flow caused by tidal processes such as Stokes' transport, tidal pumping, and tidal oscillatory flux [see e.g., *Chen et al*., 2012]. A quasi-Lagrangian approach that maps fluxes onto a salinity coordinate as outlined in *MacCready* [2011] does, however, capture the "total exchange flow" and we will therefore apply it here.

Flux in salinity coordinates is given by

$$Q(s) \equiv \left\langle \int_{A_s} u\, dA \right\rangle, \tag{11}$$

where A_s is the cross-sectional area with salinity greater than s, u is the streamwise velocity, and $\langle\cdot\rangle$ denotes a time-average operator. The inward salt flux is given by

$$F_{in} = \int_0^{s_o} s\frac{\partial Q}{\partial s}\bigg|_{in} ds, \tag{12}$$

where the subscript *in* indicates only integrating for flow directed into the estuary. Again, s_o is the ocean salinity, i.e., the upper bound of the integration. Equation (12) was computed over discrete salinity intervals of 0.5 g kg^{-1} and summing along a cross section near the estuary mouth at each model time step. The tidally averaged flux was then computed by applying a 24-25-24 h Godin-type filter.

3. Results

An overview of the estuary conditions (river discharge, freshwater fraction, and inward salt flux) from the 2009 SUNTANS simulation are shown in Figure 2. The peak in river discharge ($Q_r = 1000$–2500 m^3 s^{-1}) occurred between mid-April and mid-May 2009. Outside of this period, the discharge was generally less than 500 m^3 s^{-1}. The estuary freshwater fraction increased from 0.4 to 0.7 during the high-flow period and decreased linearly from mid-May to the end of the simulation when river flow was weak. The tidally averaged isohaline salt flux (equation (12); Figure 2d) varied between 0.1 and 0.9 $\times 10^5$ psu m^3 s^{-1} and showed no correlation with river discharge, although it was correlated with tidal strength and therefore exhibited a fortnightly modulation.

We have calculated the various estuary time scales described in the introduction starting with the Lagrangian residence time as it does not rely on assumptions about the steadiness of the forcing. Consequently, it was also the most computationally expensive. In this section, we compare the different time scales to the Lagrangian residence time in order to understand what they represent and how they relate to each other.

3.1. Lagrangian Residence Time

The spatial distributions of the monthly averaged residence time, τ_L, for April, May, and June are shown in Figure 4. Residence times were lowest (<15 days) near the mouth and San Luis Pass and increased along the Houston Shipping Channel and into Trinity Bay. During April, when river discharge was high, the residence time was less than 30 days in Trinity Bay and increased in May and June. It was greater than 45 days in parts of Trinity Bay by June coinciding with low river discharge. East and West Bays had residence times greater than 45 days for all 3 months highlighting low exchange between these regions of the estuary.

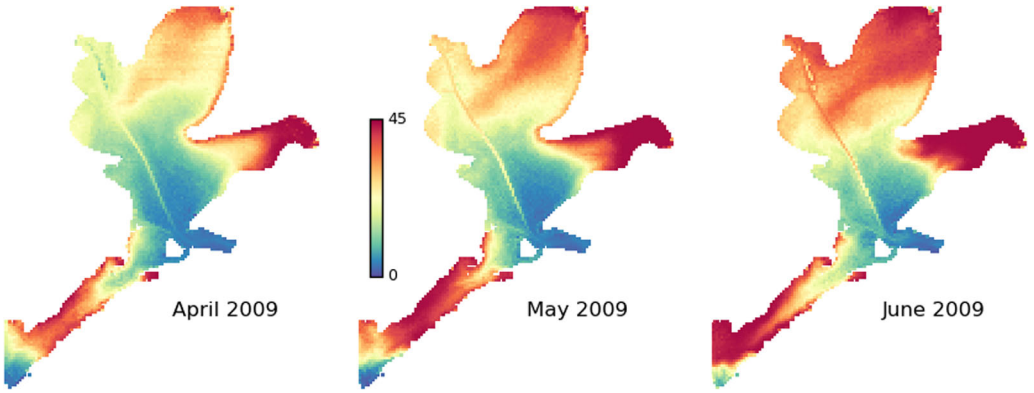

Figure 4. Monthly averaged Lagrangian residence times, τ_L (day).

The fractional distribution of the Lagrangian residence time was estimated for each particle simulation by binning $\tau_L(x_0,\ y_0)$ into one-day bins and is shown in Figure 5. The distribution shows the fraction or probability (P) of particles (volume) with a given τ_L and how that varies in time. The mean started at 30 days and then dropped to 15 days by mid-April and subsequently returned to 30 days by mid-May. During low-flow periods, the distribution was skewed toward high $\tau_L(x_0,\ y_0)$, and during high-flow toward low $\tau_L(x_0,\ y_0)$. A consequence of the skewness was that during the high-flow period, there were fewer regions with $\tau_L(x_0,\ y_0)$ greater than 30 days ($p < 0.005$), i.e., the whole system flushed. During low flow, the distribution was more heterogeneous; regions with $0 < \tau_L(x_0,\ y_0) < 5$ days fluctuated between 0.005 and 0.04 at a fortnightly period, consistent with variations in tidal forcing magnitude. These results highlight how river discharge and tidal forcing influence the residence time.

3.2. Mean Age

Mean age distributions for three different time periods are shown in Figure 6. The snapshots were taken during high river flow, postflooding when the volume-averaged salinity was still decreasing, and after the high flow when the total freshwater fraction was decreasing (salinity was increasing) (see Figure 2c). The general distribution from all three periods was young age (<15 days) in the shipping channel region, steadily increasing age in Trinity Bay (15–45 days), and old age (>60 days) in East and West Bays. Age was generally vertically stratified by 1–2 days in the shipping channel and Trinity Bay indicating the presence of

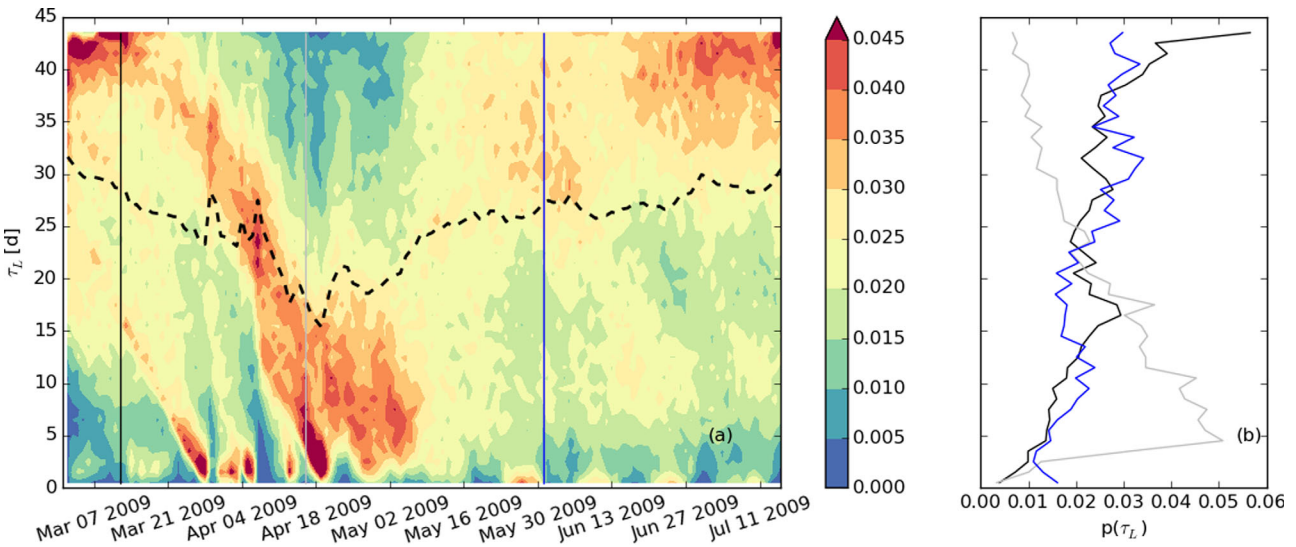

Figure 5. (a) Fractional distribution of Lagrangian residence time as a function of time. The dashed line is the mean. (b) Distribution at time periods indicated by the vertical lines in Figure 5a.

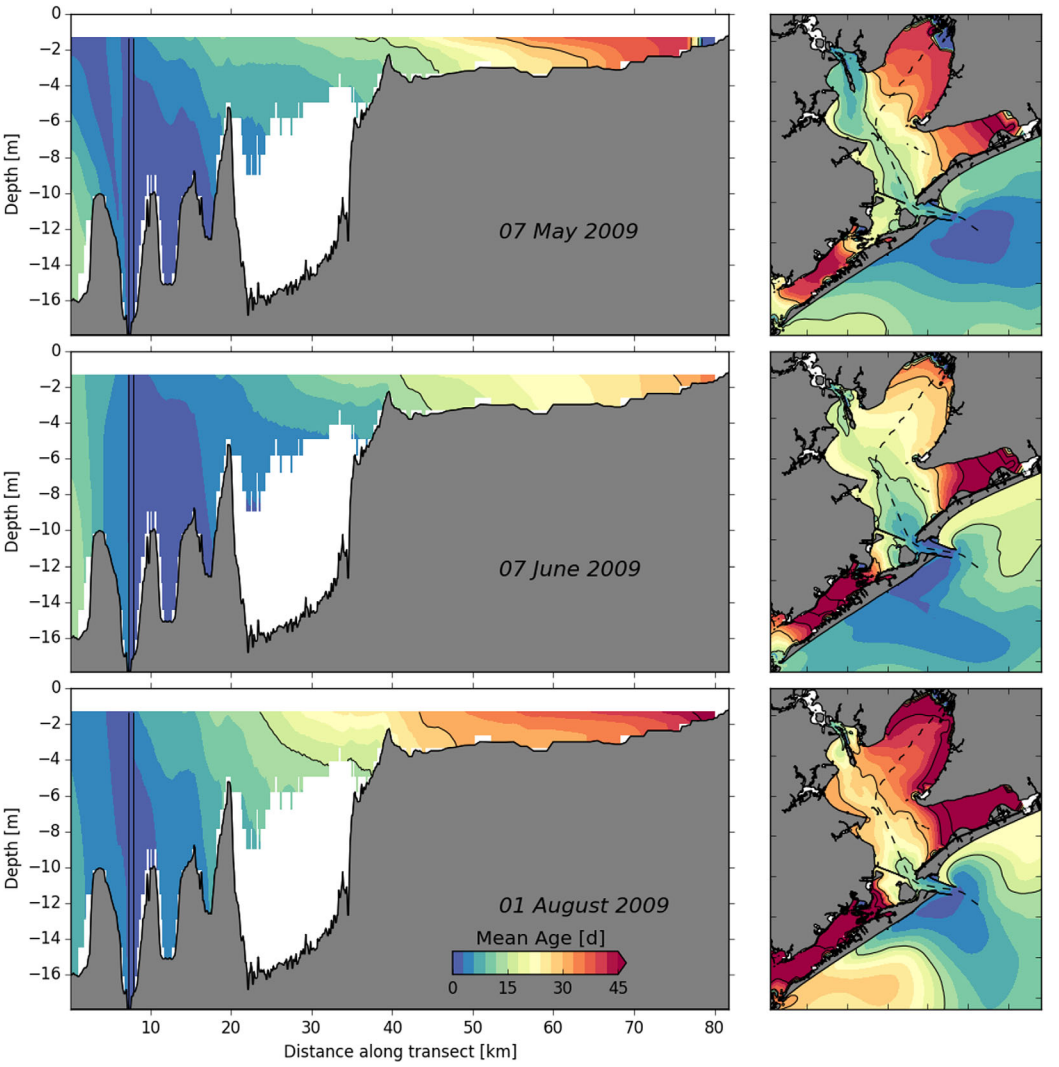

Figure 6. Example snapshots of the mean age (left) along the estuary center line and (right) at the surface for three different points in time during high discharge (7 May), immediately after (7 June), and 3 months after (1 August). The age source region is near the zero contour (x = 8 km). The centerline is given by the dashed line in the surface plots.

sheared residual circulation driving ocean (young age) water upstream near the seabed in a time-averaged sense. By definition, the age distribution in Figure 6 shows how long a water mass has taken to reach a given region. Differences between the three different monthly averages shown highlight the unsteadiness of the age due to time-variable forcing.

The fractional distribution of mean age over time is shown in Figure 7. The volume-averaged mean age increased linearly during the model spin-up period (March) but remained relatively constant at 20 days from 1 April to 1 June 2009. From 1 June to 1 September, the mean steadily increased from 20 to 40 days. Mean age distribution was mainly bimodal with a peak at 0–5 days, representing freshly exchanged gulf water, and a second peak just below the mean (15–30 days) that we will refer to as mid-age water. One exception to this bimodal distribution was following the flooding event when a peak was initially visible around 20 April at 20 days and increased linearly to 40 days by 5 May. Conceptually, this represents injection of mid-age water further into the estuary without mixing with surrounding fluid, as mixing would inhibit aging of the mean age tracer. Enhanced baroclinic circulation in the upper estuary caused by river flooding is the likely driver of this increased flux. Similar injection events occurred on a smaller scale between the zero-age Gulf and mid-age water.

Characteristic lines in the mean age fractional distribution originated near age zero and propagated linearly in time-age space shown in Figure 7. These characteristic lines represent ocean water that enters the

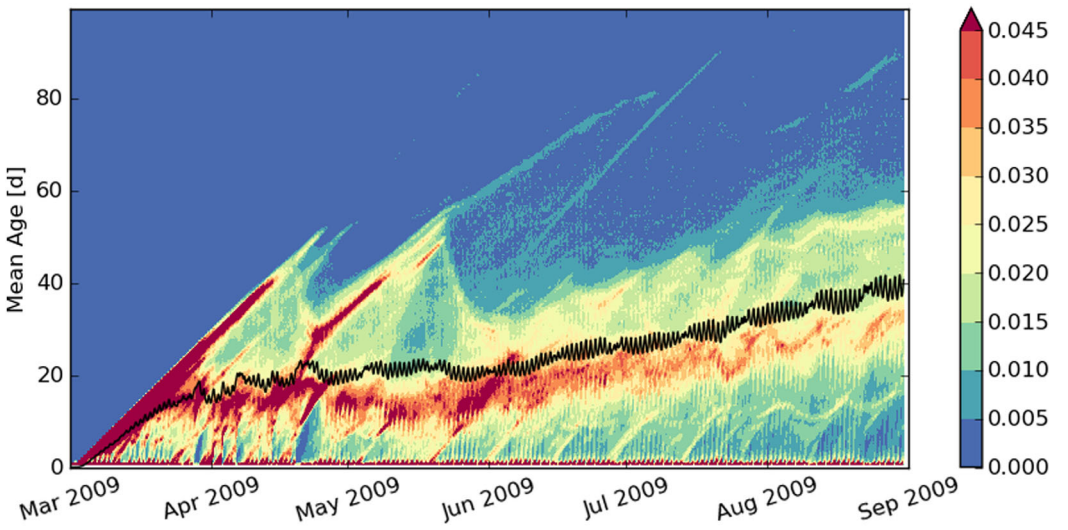

Figure 7. Fractional distribution of mean age as a function of time for Galveston Bay. The mean of the distribution is indicated by the solid black line.

estuary without mixing, and hence the mean age is given by the time since entering the estuary. The volume of fluid in a discrete age range is simply the fraction of that age multiplied by the total estuarine volume. Therefore, a characteristic line with a probability of 5% that originates at age zero represents a 5% input of "new" water into the estuary. The timing of these injection events was not regular during March and April 2009, although the injection events generally occurred during neap tides thereafter.

3.3. Particle *e*-Folding Time

As shown in Figure 8a, the particle *e*-folding time, τ_e (equation (4)), varied between 20 and 40 days between 1 April 2009 and 1 July 2009. Recall that, since 45 days of particle-tracking simulation are required for each estimate, τ_e could not be computed beyond 15 July 2009 (45 days before the end of the simulation on 1 September 2009). The flushing time decreased from 40 to 20 days by mid-April 2009 and then increased back to 40 days by mid-May. The decrease in τ_e coincided with the high river flow period.

The main limitation of the exponential decay model is that mass (particles) loss from the estuary is assumed to be due to dispersion not advection of mass by river discharge. We calculated the root-mean-square error (RMSE) between the numerically predicted fraction of particles remaining inside the bay and those predicted by using

$$RMSE(t_s) = \sqrt{\frac{\sum_{j=1}^{T_e} (N_{fit}(t_s,\ t_j) - N(t_j))^2}{T_e}}$$

where $T_e = 45$ days and $N_{fit}(t_s,\ t_j)$ is the fit from equation (4) starting at time t_s. The RMSE, shown in Figure 8c, highlights the periods when the CSTR assumption is questionable. RMSE was largest (0.11) during high river discharge (around late April) demonstrating the weakness of this approach when advection is important. Examples of the best fit line during three periods are shown in Figure 8b to demonstrate the suitability of the model fit. During high discharge periods (blue line), there was a pronounced mismatch during the initial 10 days; the particle count decayed more rapidly than the linear model predicted probably due to advection through the mouth. During low discharge (red line), the fit was good (RMSE = 0.05).

These results indicate that the CSTR model is only suitable for predicting the decay of a tracer during low discharge periods in Galveston Bay. This is likely due to the dominance of tidally driven exchange at the mouth only during periods of low discharge. Tidal exchange can be parameterized as a dispersive process and therefore the assumptions of the CSTR model are satisfied.

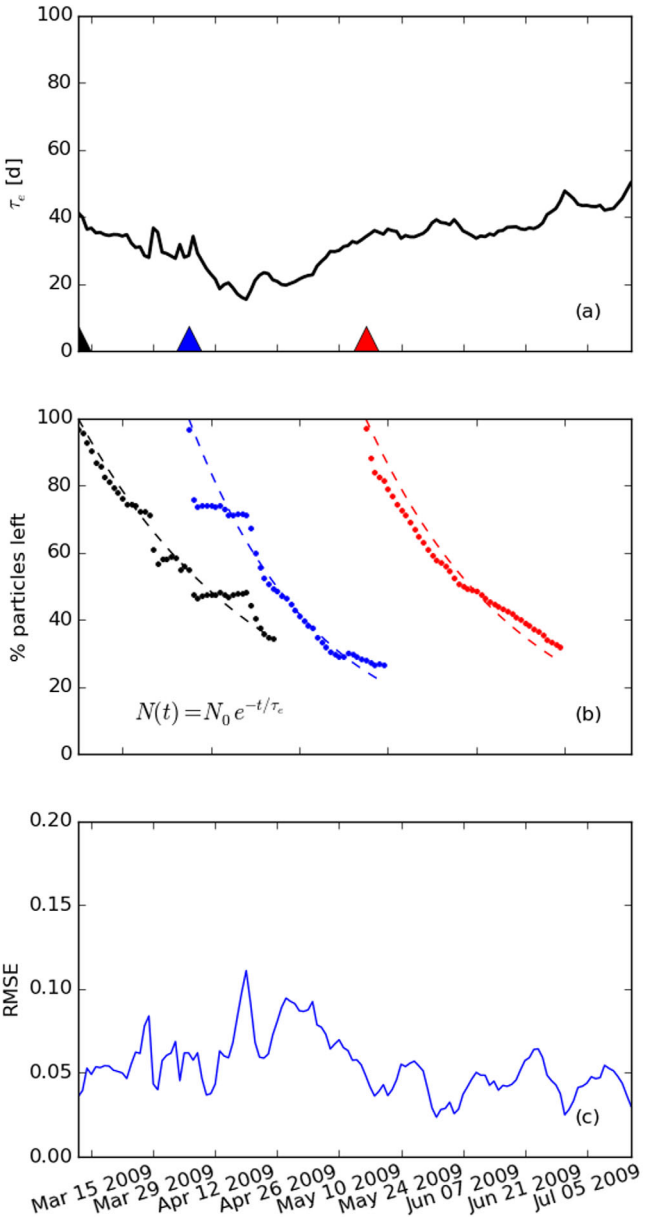

Figure 8. (a) Particle *e*-folding (flushing) time for particles initialized on each day and run for 45 days, (b) examples of best fit curves at three different initialization times indicated by the colored triangles in Figure 8a, and (c) RMSE of the best fit to an exponential decay.

3.4. Freshwater and Salinity Turnover Times

The bulk freshwater and salinity turnover time scales are shown in Figure 9. The freshwater turnover time (equation (2), Figure 9a) varied from 10 days during April 2009 when the discharge was largest to greater than 600 days during the drier months of June and July. Flushing time was mainly controlled by freshwater inflow (Figure 2b), which varied by orders of magnitude. In contrast, the freshwater fraction (Figure 2c) only varied from 0.4 to 0.6 (1.0 is completely fresh) during the high discharge period and gradually decreased to 0.25 over roughly 4 months.

The salinity turnover time, τ_T (equation (2)), is shown in Figure 9b. The salinity turnover time varied from 10 to 500 days with the largest peaks during storms when the residual inward salt flux, $\langle F_{in} \rangle$, approached zero (see Figure 2d). From May onward, the salinity turnover time exhibited a fortnightly modulation concomitant with variations in tidal forcing and varied between 10 and 40 days. There was little to no correlation between the turnover time and river forcing because the inward salt flux, $\langle F_{in} \rangle$, responded very weakly to the river discharge.

4. Discussion

4.1. Unsteadiness

The freshwater turnover time τ_f (equation (2)) and the salinity turnover time τ_T (equation (3)) are the most computationally efficient time scales to estimate. However, both of these bulk time scales assume that the system is in steady state, i.e., the mass of salt in the estuary is constant. The volume-integrated freshwater fraction *f* (equation (1)) showed that the system was constantly adjusting over the time period investigated here (see Figure 9b). A steady state assumption may be satisfied given a suitable averaging time that is much greater than the tidal period used to compute the salt fluxes. *MacCready and Geyer* [2001] formally show that steady state is satisfied over an averaging period *T* if

$$\gamma_f = \frac{|\Delta V_{fw}|/T}{\bar{Q}_r^T} \ll 1\,, \tag{13}$$

where $\Delta V_{fw} = \int_V f(T)\ dV - \int_V f(0)\ dV$ is the freshwater volume change, and $\bar{Q}_r^T = \int_0^T Q_r(t')dt'/T$ is the average river flow over the time period, *T*. We define γ_f as the freshwater unsteadiness term. In a similar manner, we may use salinity fluxes instead of freshwater as in equation (13) to give

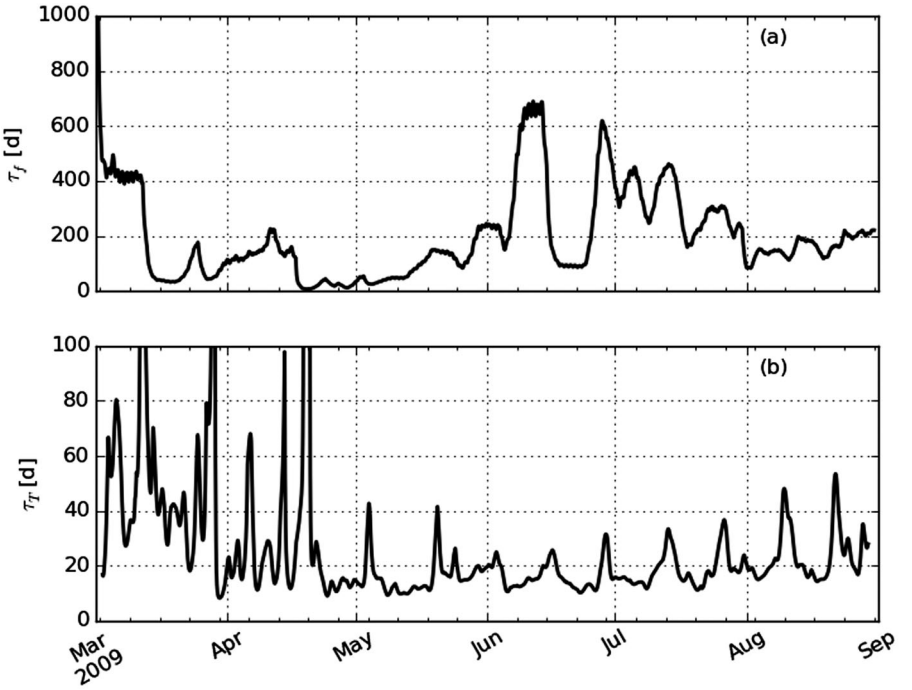

Figure 9. (a) The freshwater turnover time τ_f from equation (2), and (b) salinity turnover time τ_T from equation (3) for the 2009 simulation period. Note that the turnover time goes off scale in March and April 2009.

$$\gamma_s = \frac{|\Delta \bar{s}^{xyz}|/T}{\bar{F}_{in}^{T}} \ll 1\,, \tag{14}$$

where $\bar{s}^{xyz}$ is the volume-averaged salinity, $\Delta \bar{s}^{xyz} = \bar{s}^{xyz}(T) - \bar{s}^{xyz}(0)$, and $\bar{F}_{in}^{T} = \int_0^T F_{in}(t')dt'/T$.

The two unsteadiness parameters, shown in Figure 10, give a suitable time scale, T, over which conditions in equations (13) and (14) are satisfied and provide an estimate of the time period needed to assume steadiness. The salinity unsteadiness parameter was < 0.1 for $T = 18$ days, while the freshwater parameter was

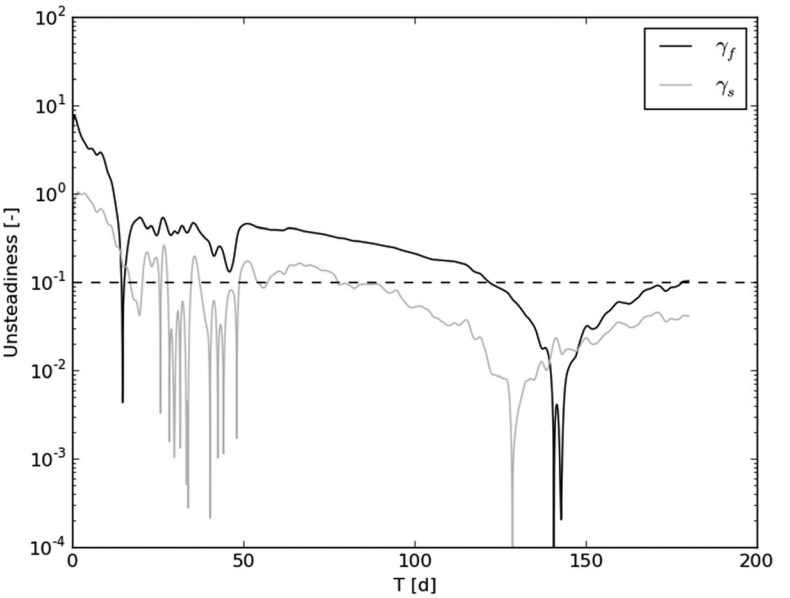

Figure 10. Freshwater and salinity unsteadiness parameters as defined in equations (13) and (14), respectively.

closer to 120 days indicating that the estuary was unsteady and took longer to respond than the time scales of the forcing. This implies that the isohaline flux needs to be averaged over 18 days or more to compute a meaningful salinity turnover time τ_T using equation (3). Furthermore, the steadiness time for freshwater fluxes indicated that the estuary could only be assumed to be in equilibrium if flow remained constant over semiannual time scales. We therefore recomputed the salinity flux using a longer averaging period and discuss the results below.

4.2. Unsteady Particle Flushing Model

The main flaw of the CSTR model for calculating flushing time with particles presented in section 3.3 is that the exchange is assumed to be a steady process and therefore a decay model like equation (4) only applies under those circumstances. An alternative flushing model that incorporates the unsteady properties of the system, i.e., the river discharge, is therefore desirable. Here we will provide details of a model that incorporates the time-variable river flow into the flushing calculation.

The particle concentration for an estuary of volume V is given by

$$\frac{d\bar{N}}{dt} = Q_{in}\bar{N}_{in} + Q_{out}\bar{N}_{out}, \tag{15}$$

where $\bar{N} = N/V$ is the particle concentration, $\bar{N}_{in}$ and $\bar{N}_{out}$ are the inflowing and outflowing particle concentrations, and Q_{in} and Q_{out} are the net (residual) exchange flows into and out of the estuary, respectively. Next we assume that the inflowing particle concentration, $\bar{N}_{in}$, is zero, which is reasonable given the number of particles returning into the system was negligible. Using conservation of volume

$$Q_{in} + Q_{out} = -Q_r\,, \tag{16}$$

and assuming $\bar{N}_{out} \approx \bar{N}$ gives

$$\frac{d\bar{N}}{dt} = -(Q_r(t) + Q_{in})\bar{N}, \tag{17}$$

noting that the river flow $Q_r(t)$ is time dependent. The solution to (17) is given by

$$\bar{N}(t) = N_0 \exp\left(-\int_0^t \frac{Q_r(t') + Q_{in}}{V}\, dt'\right), \tag{18}$$

where N_0 is the initial total number of particles, not concentration. We now have one unknown, Q_{in}, that we find by least squares fitting equation (18) using the known river discharge and $\bar{N}(t)$ from each particle simulation. The relevant time scale is now $\tau = V/Q_{in}$.

Note that under constant discharge conditions, (18) is equivalent to the CSTR model, i.e.,

$$\bar{N}(t) = N_0 \exp\left(-\frac{Q_r + Q_{in}}{V} t\right), \tag{19}$$

noting that

$$\frac{Q_r + Q_{in}}{V} \equiv \frac{1}{\tau_e}. \tag{20}$$

The least squares fit to equation (18) is shown in Figure 11. The time scale, $\tau = V/Q_{in}$, was roughly 10–20% lower than the CSTR model value (Figure 8). The unsteady flushing model was also able to capture some of the transient features in the particle flushing curves caused by variable river flow (Figure 11b). The benefits of the unsteady particle flushing model are that it highlights the influence of the time history of river flow and it separates river and exchange flow-driven flushing into different terms.

4.3. Summary of Time Scales

Figure 12 summarizes all of the time scales on one plot, where we have used the bulk volume-averaged Lagrangian residence time, $\bar{\tau}_L^{xyz}$, and bulk mean age, $\bar{a}^{xyz}$, as representative values for these spatially varying quantities. We recalculated the salinity turnover time τ_T (equation (3)) using an averaging period of 18 days and it was far less variable and was roughly half of the Lagrangian residence time $\bar{\tau}_L^{xyz}$. The Lagrangian residence time and particle e-folding time τ_e followed a similar trend with a minimum during peak discharge,

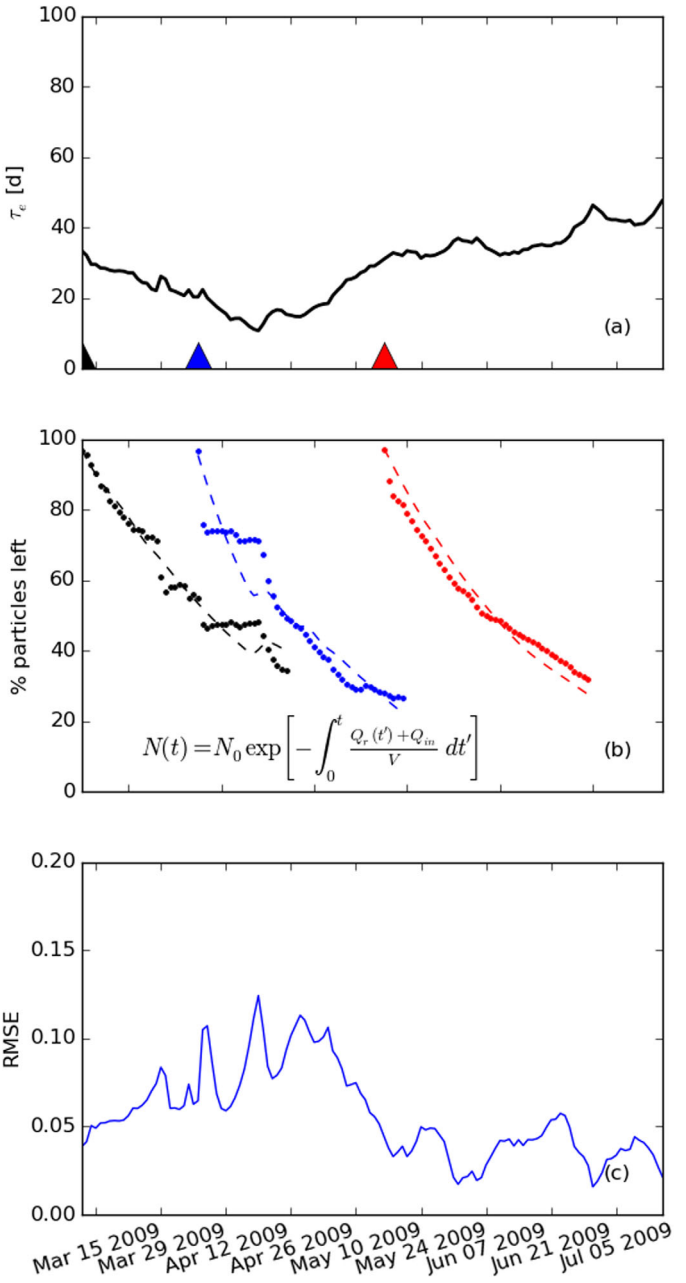

Figure 11. (a) Particle flushing time for scenarios initialized at daily intervals, (b) examples of best fit curves at three different initialization times indicated by the colored triangles in Figure 11a, and (c) RMSE of the best fit to equation (18).

although the *e*-folding time was roughly 30% longer. The volume-averaged mean age $\bar{a}^{xyz}$, however, plateaued during peak discharge and grew linearly in time from June onward. All four time scales were between 20 and 50 days and were roughly equal (20 days) during peak river flow. Interestingly, the turnover time was approximately equal to the time scale T required to satisfy a steady state assumption.

Similar to *Kranenburg* [1986] and *Hetland and Geyer* [2004], we have used the freshwater advective time, $\tau_h = V/Q_r$ to normalize each time scale (Figure 12b). All four time scales were equal to each other and to τ_h during the high-flow period (mid-April). During low-flow periods, the time scales were 2–100 times smaller than the freshwater advective time. One implication of this result is that previously reported transport time scales based on annual average discharge [e.g., *Santschi*, 1995] are likely too long. Transport time scales are only equal to the advective time scale during high discharge periods.

Hetland and Geyer [2004] refer to the ratio τ_h/τ as a speedup factor. They conclude that a speedup factor of unity implies that salinity adjustment is purely due to advection since a freshwater parcel traverses the length of the estuary over a time scale that is inversely proportional to the river inflow velocity, $u_r \sim Q_r/A$, where A is a representative cross-sectional area of the estuary. When the speedup factor is much greater than one, salt adjustment is dominated by exchange flow. Similar conclusions can be drawn about the adjustment time in Galveston Bay: during the flooding period, salinity responded to river discharge at the same rate as the replacement time. However, during low-flow conditions, the adjustment time was much shorter.

4.4. Relationship With Freshwater Advective Time

The different time scales are plotted against the freshwater advective time, τ_h, in Figure 13. All time scales were normalized by the minimum freshwater advective time, $\tau_{min} \approx 15$ days ($Q_r = 2800$ m^3 s^{-1}), so that the values converged to one during maximum river flow. The volume-averaged mean age and Lagrangian residence time, as well as the Lagrangian flushing time all followed a linear trend with τ_h in log-space. The salinity turnover time did not, however, exhibit any linear trend and instead showed some time lag effects.

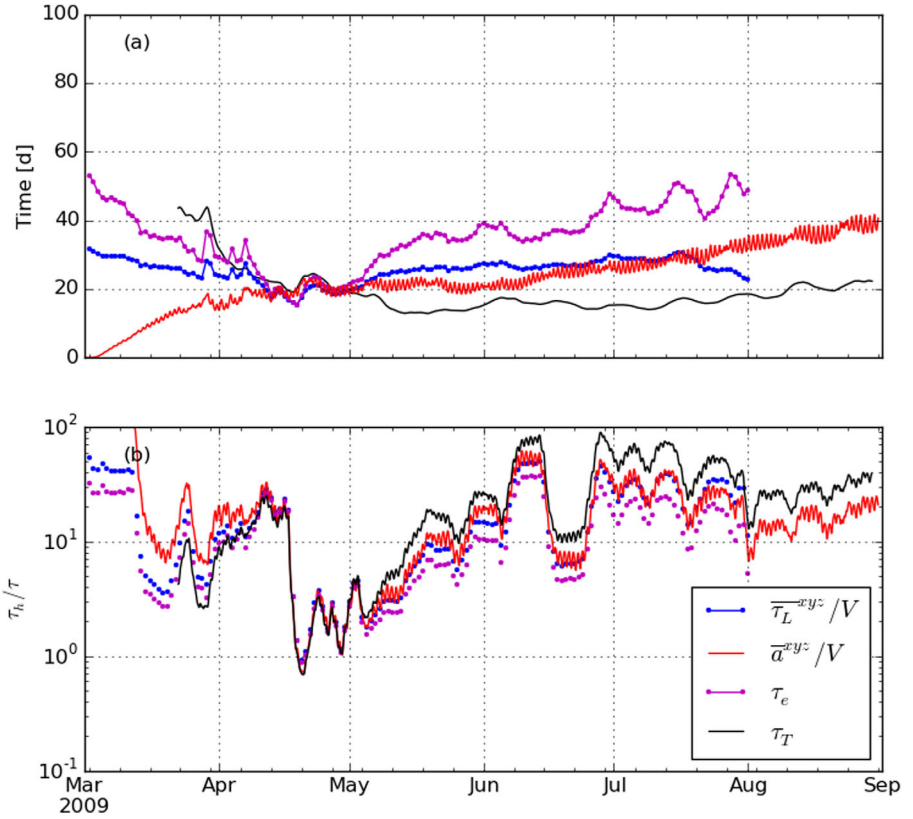

Figure 12. Comparison of the volume-averaged Lagrangian residence time, volume-averaged age, particle flushing time, and salinity turnover time normalized by the freshwater advective time.

The linear trend in log-space suggests that three of the time scales have a dependence on the τ_h (and river flow) given by

$$\frac{\tau}{\tau_{min}} = b\left(\frac{\tau_h}{\tau_{min}}\right)^{\gamma}, \qquad (21)$$

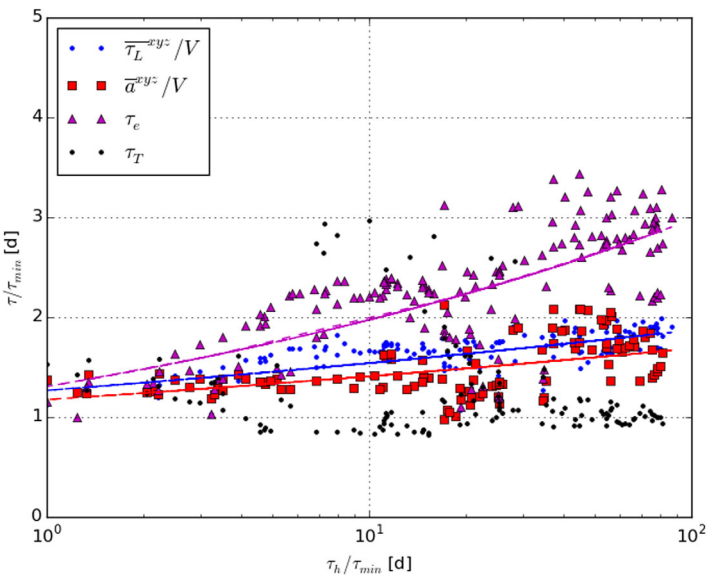

Figure 13. Normalized time scales plotted against the normalized freshwater advective time, τ_h.

where b represents the time scale at minimum τ_h and γ indicates the sensitivity to τ_h and hence river flow; $\gamma = 1$ indicates that river flow (advection) dictates the time scales under all conditions whereas $\gamma < 1$ indicates increasing importance of diffusive processes driving tracer exchange. The value of b for all fits in Figure 13 was roughly unity indicating that these time scales equal the flushing time during high flow. For τ_e, γ=0.18, while γ=0.08 for the volume-averaged mean age and residence time. This implies a greater sensitivity of τ_e to river flow than the mean age and residence time.

Lemagie and Lerczak [2014] investigated the sensitivity of the tracer turnover time and particle flushing time using idealized hydrodynamic scenarios of Yaquina Bay, Oregon. Using a slightly different methodology than that described here, they showed that particle flushing time was more sensitive to river flow than the tracer turnover time and concluded that the tracer turnover time was not representative of transport in that particular system. In our unsteady case, we found little relationship between river flow and τ_T, although we found that the particle flushing was more sensitive to river flow than the bulk mean-age and Lagrangian residence time. This reduced sensitivity is probably due to tidal trapping/pumping mechanisms controlling these time scales, and that these mechanisms are not as sensitive to freshwater flow.

The lack of a relationship between the salinity turnover time τ_T and τ_h is likely due to time-dependent effects not being accounted for in the calculation of τ_T via equation (3). The bulk mean age and Lagrangian time scales implicitly account for flow history and are therefore less sensitive to transient effects, whereas τ_T is entirely dependent on the instantaneous total exchange flow at the mouth, F_{in}. We conclude that bulk time scales like τ_T and τ_f do not give a representative time scale in highly unsteady estuaries subject to realistic forcing.

4.5. Application to Oil Spill Transport

In the context of an oil spill within the estuary, oil transport can be quite complex owing to numerous chemical factors that impact its buoyancy [*Reed et al.*, 1999]. However, time scales related to neutrally buoyant particles or passive tracers reveal information about the dominant transport time scales that would be expected in the event of an oil spill. In this regard, the Lagrangian residence time is most useful for understanding potential impacts of oil spills. Bulk transport time scales have limited applicability because they do not reveal information about spatial variability of the residence time. Observations from the Texas City "Y" spill revealed that oil departed the mouth of the estuary within a few hours. This was likely due to numerous factors, including the fact that the spill occurred close to the entrance, over a short duration, on the ebb phase of the tide, and during a north-easterly wind. These factors combined to flush the oil from the system fairly rapidly. Maps of the Lagrangian residence time (Figure 4) revealed that oil released close to the mouth would exit the bay within 2–3 days, although oil released further into the estuary, such as Baytown, would take longer. Freshwater and salinity turnover time scales were by contrast on the order of 10 days. Results also showed that τ_L is river flow dependent, therefore an oil release in Trinity Bay during high discharge (April) would take 20–30 days to flush, whereas during low discharge (June) it would take longer than 40 days. These general trends are also applicable to other Gulf Coast estuaries, which have similar physical characteristics as Galveston Bay, although the exact time scales would vary.

5. Conclusions

There are various time scales used to characterize the rate that material is circulated through an estuary. Here we have used a three-dimensional hydrodynamic model to calculate several different time scales for Galveston Bay during a time period when the system was subject to transient forcing. The flushing rates of lagoons and estuaries subject to transient freshwater inflow are not as well studied [see e.g., *Largier*, 2010]. Estuaries along the Gulf of Mexico coastline reside in this category due to the rainfall climatology of the region.

For Galveston Bay, during March–September 2009, the Lagrangian flushing time was the largest of the time scales and varied from 20 to 50 days. The volume-averaged Lagrangian residence time and mean age were approximately equal from mid-April to August with a range of 20 to 30 days. The mean age increased to 40 days between August and September. Salinity turnover time, calculated with an 18 day running average for the inward salt flux, peaked at roughly 40 days prior to the high discharge event and then decreased to 15 days during the postflooding period. These results indicated that the salinity turnover time was too short likely because the centroid of salt mass in the estuary was closer to the inlet than the centroid of the water volume. Based on these results, 20–40 days is a suitable measure for the tracer exchange time scale for Galveston Bay under typical conditions. Note, however, that we have not investigated these time scales under extreme conditions such as 2011 when there was a prolonged drought, or early 2015 when there was flooding across southern Texas.

The Lagrangian residence time, which relies on no assumptions about the steadiness or the tracer homogeneity within the system, provided a reference scale with which to compare the other time scales. Although it exhibited significant spatial and temporal variability in a time-averaged sense, it decreased from the estuary mouth to the river and temporally with river discharge. The mean age showed similar spatial and temporal trends as the Lagrangian residence time and the volume-averaged values of τ_L and a were approximately equal throughout the time period investigated here. Given the increased numerical cost of computing the Lagrangian residence time, we can conclude that the mean age is a more efficient metric for characterizing an unsteady estuary. Both the age and residence time do not rely on a steady state assumption and were therefore useful time scale metrics even under transient forcing conditions when the river discharge varied by orders of magnitude.

The salinity turnover time, calculated using an isohaline flux decomposition (TEF), was within $\pm$50% of the Lagrangian residence time as long as a suitable averaging time was chosen so as to satisfy the steady state assumption. The difference between the salinity turnover time and the mean Lagrangian residence time indicated that not all of the tracer exchanged at the mouth was mixed throughout the system. An additional adjustment factor is therefore necessary to compensate for the violation of the well-mixed assumption.

All time scales collapsed onto the same value of roughly 20 days during the high-flow period indicating that advection dominated the flushing and turnover of the system during this period. During low-flow periods, the time scales diverged, which was probably due to the contribution of different dispersive processes acting in different regions of the estuary. This minimum flushing time of roughly 20 days shows the approximate response time of Galveston Bay to a variation in forcing, e.g., the signature of a transient high-flow event will remain in the system at least 20 days afterward.

Finally, the volume-averaged Lagrangian residence time, mean age, and the Lagrangian flushing time scaled with τ_h^{γ}, where for Galveston Bay $\gamma = 0.08$–0.18. The low value of γ indicates low sensitivity to river discharge for this system. In general, the relationship highlights that integrated time scales calculated using particles or an age tracer are predictable based on river flow alone even in a realistic, time-dependent estuary.

Acknowledgments

This research was made possible by a grant from The Gulf of Mexico Research Initiative. Numerical model data are publicly available through the Gulf of Mexico Research Initiative Information & Data Cooperative (GRIIDC) at https://data.gulfresearchinitiative.org/data/R1.x137.108:0004. We thank three anonymous reviewers for their helpful suggestions on an earlier version of this manuscript.

References

Banas, N. S., and B. M. Hickey (2005), Mapping exchange and residence time in a model of Willapa Bay, Washington, a branching, macrotidal estuary, *J. Geophys. Res.*, *110*, C11011, doi:10.1029/2005JC002950.

Bolin, B., and H. Rodhe (1973), A note on the concepts of age distribution and transit time in natural reservoirs, *Tellus*, *1*(258), 58–62.

Casulli, V., and P. Zanolli (2005), High resolution methods for multidimensional advectiondiffusion problems in free-surface hydrodynamics, *Ocean Modell.*, *10*(1-2), 137–151, doi:10.1016/j.ocemod.2004.06.007.

Chen, S., W. Geyer, D. Ralston, and J. Lerczak (2012), Estuarine exchange flow quantified with isohaline coordinates: Contrasting long and short estuaries, *J. Phys. Oceanogr.*, *42*(5), 748–763, doi:10.1175/JPO-D-11-086.1.

Chua, V. P., and O. B. Fringer (2011), Sensitivity analysis of three-dimensional salinity simulations in North San Francisco Bay using the unstructured-grid SUNTANS model, *Ocean Modell.*, *39*(3-4), 332–350, doi:10.1016/j.ocemod.2011.05.007.

Deleersnijder, E., J. M. Campin, and E. J. M. Delhez (2001), The concept of age in marine modelling I. Theory and preliminary model results, *J. Mar. Syst.*, *28*(3-4), 229–267.

Delhez, E. J., J.-M. Campin, A. C. Hirst, and E. Deleersnijder (1999), Toward a general theory of the age in ocean modelling, *Ocean Modell.*, *1*(1), 17–27.

Fischer, H. B., E. J. List, R. C. Y. Koh, J. Imberger, and N. H. Brooks (1979), *Mixing in Inland and Coastal Waters*, vol. 114, pp. 315–316, Academic Press, San Diego, Calif., doi:10.1017/S002211208223028X.

Fringer, O. B., M. Gerritsen, and R. L. Street (2006), An unstructured-grid, finite-volume, nonhydrostatic, parallel coastal ocean simulator, *Ocean Modell.*, *14*, 139–173.

Gonzalez, L. A., and L. J. Lester (2011), State of the bay: A characterization of the Galveston Bay ecosystem, Third Edition, Texas Commission on Environmental Quality, Galveston Bay Estuary Program, 356 pp., Houston, Tex. [Available at http://www.galvbaydata.org/StateoftheBay/tabid/1846/Default.aspx.]

Hetland, R. D., and W. Geyer (2004), An idealized study of the structure of long, partially mixed estuaries, *J. Phys. Oceanogr.*, *34*, 2677–2691.

Ketefian, G. S., E. S. Gross, and G. S. Stelling (2016), Accurate and consistent particle tracking on unstructured grids, *Int. J. Numer. Methods Fluids*, *80*(11), 648–665, doi:10.1002/fld.4168.

Kranenburg, C. (1986), A time scale for long-term salt intrusion in well-mixed estuaries, *J. Phys. Oceanogr.*, *16*, 1329–1331.

LaBolle, E. M., J. Quastel, and G. E. Fogg (1998), Diffusion theory for transport in porous media: Transition-probability densities of diffusion processes corresponding to advection-dispersion equations, *Water Resour. Res.*, *34*, 1685–1693, doi:10.1029/98WR00319.

Largier, J. (2010), Low-inflow estuaries: Hypersaline, inverse and thermal scenario, in *Contemporary Issues in Estuarine Physics*, edited by A. Valle-Levinson, chap. 9, pp. 247–272, Cambridge Univ. Press, N. Y.

Lemagie, E. P., and J. A. Lerczak (2014), A comparison of bulk estuarine turnover timescales to particle tracking timescales using a model of the Yaquina Bay Estuary, *Estuaries Coasts*, *38*, 1797–1814, doi:10.1007/s12237-014-9915-1.

Lucas, L. V. (2010), Implications of estuarine transport for water quality, in *Contemporary Issues in Estuarine Physics*, pp. 273–307, Cambridge Univ. Press, N. Y., doi:10.1029/2003JD004173.

MacCready, P. (2011), Calculating estuarine exchange flow using isohaline coordinates, *J. Phys. Oceanogr.*, *41*(6), 1116–1124, doi:10.1175/2011JPO4517.1.

MacCready, P., and W. Geyer (2001), Estuarine salt flux through an isohaline surface, *J. Geophys. Res.*, *106*, 629–637.

Mesinger, F., et al. (2006), North American regional reanalysis, *Bull. Am. Meteorol. Soc.*, *87*(3), 343–360, doi:10.1175/BAMS-87-3-343.

Monsen, N., J. Cloern, L. Lucas, and S. Monismith (2002), A comment on the use of flushing time, residence time, and age as transport time scales, *Limnol. Oceanogr.*, *47*(5), 1545–1553.

Postma, L., J. K. L. van Beek, H. F. P. van den Boogaard, and G. S. Stelling (2013), Consistent and efficient particle tracking on curvilinear grids for environmental problems, *Int. J. Numer. Methods Fluids*, *71*, 1226–1237, doi:10.1002/fld.3705.

Rayson, M. D., E. S. Gross, and O. B. Fringer (2015), Modeling the tidal and sub-tidal hydrodynamics in a shallow, micro-tidal estuary, *Ocean Modell.*, *89*, 29–44, doi:10.1016/j.ocemod.2015.02.002.

Reed, M., O. I. Johansen, P. J. Brandvik, P. Daling, A. Lewis, R. Fiocco, D. Mackay, and R. Prentki (1999), Oil spill modeling towards the close of the 20th century: Overview of the State of the Art, *Spill Sci. Technol. Bull.*, *5*(1), 3–16, doi:10.1016/S1353-2561(98)00029-2.

Roelke, D. L., H. P. Li, N. J. Hayden, C. J. Miller, S. E. Davis, A. Quigg, and Y. Buyukates (2013), Co-occurring and opposing freshwater inflow effects on phytoplankton biomass, productivity and community composition of Galveston Bay, USA, *Mar. Ecol. Prog. Ser.*, *477*, 61–76, doi:10.3354/meps10182.

Santschi, P. H. (1995), Seasonality in nutrient concentrations in Galveston Bay, *Mar. Environ. Res.*, *40*(4), 337–362, doi:10.1016/0141-1136(95)92644-J.

Schoenbaechler, C., and C. G. Guthrie (2012), Coastal hydrology for the Trinity-San Jacinto Estuary, technical report, Tex. Water Dev. Board, Austin. [Available at http://www.twdb.texas.gov/surfacewater/bays/major_estuaries/trinity_san_jacinto/doc/TWDB_Hydrology_Galveston_20120105.pdf.]

Sheldon, J., and M. Alber (2006), The calculation of estuarine turnover times using freshwater fraction and tidal prism models: A critical evaluation, *Estuaries Coasts*, *29*(1), 133–146.

Solis, R., and G. Powell (1999), Hydrography, mixing characteristics and residence times, in *Biogeochemistry of Gulf of Mexico Estuaries*, edited by T. S. Bianchi, J. R. Pennock, and R. R. Twilley, pp. 29–61, John Wiley.

Takeoka, H. (1984), Fundamental concepts of exchange and transport time scales in a coastal sea, *Cont. Shelf Res.*, *3*(3), 311–326.

Tartinville, B., E. Deleersnijder, and J. Rancher (1997), The water residence time in the Mururoa atoll lagoon: Sensitivity analysis of a three-dimensional model, *Coral Reefs*, *16*, 193–203.

Zhang, W. G., J. L. Wilkin, and O. M. E. Schofield (2010), Simulation of water age and residence time in New York bight, *J. Phys. Oceanogr.*, *40*(5), 965–982, doi:10.1175/2009JPO4249.1.